J. Fluid Mech. (1976), *vol.* 78, *part* 2, *pp.* 355–383
Printed in Great Britain

Investigation of the stability of boundary layers by a finite-difference model of the Navier–Stokes equations

By H. FASEL
Institut A für Mechanik, Universität Stuttgart, Germany

(Received 11 August 1975 and in revised form 25 May 1976)

The stability of incompressible boundary-layer flows on a semi-infinite flat plate and the growth of disturbances in such flows are investigated by numerical integration of the complete Navier–Stokes equations for laminar two-dimensional flows. Forced time-dependent disturbances are introduced into the flow field and the reaction of the flow to such disturbances is studied by directly solving the Navier–Stokes equations using a finite-difference method. An implicit finite-difference scheme was developed for the calculation of the extremely unsteady flow fields which arose from the forced time-dependent disturbances. The problem of the numerical stability of the method called for special attention in order to avoid possible distortions of the results caused by the interaction of unstable numerical oscillations with physically meaningful perturbations. A demonstration of the suitability of the numerical method for the investigation of stability and the initial growth of disturbances is presented for small periodic perturbations. For this particular case the numerical results can be compared with linear stability theory and experimental measurements. In this paper a number of numerical calculations for small periodic disturbances are discussed in detail. The results are generally in fairly close agreement with linear stability theory or experimental measurements.

1. Introduction

The stability of boundary-layer flows on a flat plate and the transition to turbulence have been the subjects of extensive studies for many years. Nevertheless, there still exist a great many unsolved problems which call for a broadening of the understanding of many aspects of laminar–turbulent transition in boundary-layer flows. According to a survey paper by Stuart (1965) the transition process can be conceived as six successive stages distinctly observable in physical experiments.

For the first stage of the transition process, namely the development of two-dimensional Tollmien–Schlichting waves, linear stability theory has been widely successful in predicting conditions for which the flow is unstable to periodic disturbances. The applicability of linear stability theory was verified by the well-known experiments of Schubauer & Skramstad (1948), thus establishing this theory as a solid basis for use in transition studies. However, these experiments also clearly laid bare the limits of linear stability theory for the understanding

of the entire transition process. Mechanisms and phenomena, following the amplification of the Tollmien–Schlichting waves and finally leading to the fully developed turbulent flow, cannot be explained by this theory. The flow takes on an increasingly three-dimensional behaviour when nonlinear effects play a more and more dominant role. Relatively few theoretical models exist (for example, Benney & Lin 1960; Greenspan & Benney 1963) and moreover are only applicable to qualitative conclusions for individual phenomena of the laminar–turbulent transition process. Today, the theoretical understanding of transition still lags far behind the experimental observations. Even for the first stage of the transition process a strengthening of the theoretical basis is required. In linear stability theory a reformulation of the Orr–Sommerfeld equation for the case of space-amplified disturbances and numerical solutions thereof (Wazzan, Okamura & Smith 1968; Jordinson 1970) have enabled direct comparison of the results with experimental measurements. However, there still remain many open questions. For example, the effects of higher harmonic wave components as well as of finite disturbance amplitudes have not been elucidated and the influence of increasing boundary-layer thickness also calls for further study. Investigations of this nature based on stability-theory analysis become extremely intricate, as was demonstrated, for example, by Bouthier (1972, 1973) and Gaster (1974) in their investigations of the influence of growing boundary-layer thickness.

The present work is an attempt to investigate the stability of laminar incompressible boundary layers and the initial phase of the transition process by direct numerical solution of the partial differential equations that describe such flow phenomena. The established boundary-layer flow on a semi-infinite flat plate is disturbed by forced time-dependent perturbations; then the reaction of this flow, i.e. the temporal and spatial development of the perturbations, is determined by numerical solution of the Navier–Stokes equations. The numerical model is restricted to two-dimensional flows and is therefore only valid as long as two-dimensional effects are dominant in the physical flow. Therefore, the present approach is mainly applicable to the investigation of the first stage of transition. In principle, extension to three space dimensions is possible, although the numerical complexity and thus the required computation times would then increase immensely. This approach to the investigation of the stability of boundary-layer flows is entirely different from the classical linear stability theory, which is restricted to periodic disturbances of small amplitudes. Here, no restriction on the form or the intensity of the disturbances is required since the ensuing development of the perturbations is described by the Navier–Stokes equations and no linearization is made anywhere.

In this paper only investigations with periodic disturbances of small amplitudes are discussed. They are compared with linear stability theory, as well as with measurements of the experiments by Schubauer & Skramstad (1948) and Ross *et al.* (1970), which were also restricted to periodic disturbances of small amplitudes. The main difficulties of this approach arise from the complicated nature of the Navier–Stokes equations, which are nonlinear and of fourth order. To date, exact closed-form solutions have been achieved only for a few relatively simple flow problems. Numerical solutions, mainly employing finite-difference methods,

have been attempted for a variety of more complicated flows, but the numerical approach can become rather involved, even for steady flows. Therefore, more and more refined methods and advanced computer systems are required. Difficulties increase when calculations of unsteady flows are attempted. Most numerical schemes, although treating the complete Navier–Stokes equations for unsteady flows, tend to smear the unsteady transient behaviour and thus yield accurate results only for large times when the flow has essentially reached a steady state. In numerically calculated unsteady flows, undesirable effects are frequently caused by the excessive artificial viscosity inherent in many popular difference schemes (Roache 1972). The present work requires the calculation of the extremely unsteady flow fields that arise from the time-dependent perturbations which are constantly introduced into the flow field. Therefore, the critical task was the development of a finite-difference method that would yield a realistic resolution of the time-dependent flow character. Moreover, for this investigation, numerical stability for the finite-difference method was a fundamental prerequisite in order to eliminate possible spurious oscillations which might arise from a numerical instability, interfere with the physically meaningful disturbances, and thus render the numerical results meaningless.

2. Governing equations

The flow phenomena to be investigated are described by the complete Navier–Stokes equations for two-dimensional laminar incompressible flows. For the numerical method the Navier–Stokes equations are used in vorticity-transport form (Schlichting 1965)

$$\frac{\partial \omega}{\partial t}+u\frac{\partial \omega}{\partial x}+v\frac{\partial \omega}{\partial y}=\frac{1}{Re}\frac{\partial^2 \omega}{\partial x^2}+\frac{\partial^2 \omega}{\partial y^2}, \tag{1}$$

with vorticity defined as

$$\omega = \partial u/\partial y-(Re)^{-1}\,\partial v/\partial x, \tag{2}$$

and the continuity equation is

$$\partial u/\partial x+\partial v/\partial y = 0, \tag{3}$$

where u and v are the velocity components in the x and y directions respectively, the co-ordinate system being defined in figure 2. All variables in (1) to (3) are dimensionless and are related to their dimensional counterparts, denoted by bars, as follows

$$x = \bar{x}/L, \quad y = \bar{y}(Re)^{\frac{1}{2}}/L, \quad t = \bar{t}U_\infty/L, \quad u = \bar{u}/U_\infty, \tag{4}$$
$$v = \bar{v}(Re)^{\frac{1}{2}}/U_\infty, \quad \omega = \bar{\omega}L/U_\infty(Re)^{\frac{1}{2}}, \quad Re = U_\infty L/\nu,$$

where L is a characteristic length, U_∞ the free-stream velocity and Re a Reynolds number (ν kinematic viscosity). The y co-ordinate and velocity component are stretched by a factor $(Re)^{\frac{1}{2}}$ to ensure that, in the numerical operations, both co-ordinates and both velocity components are of the same order of magnitude. For the calculation of the velocity components u and v the two partial differential equations

$$(Re)^{-1}\,\partial^2 u/\partial x^2+\partial^2 u/\partial y^2 = \partial \omega/\partial y, \tag{5}$$

$$(Re)^{-1}\,\partial^2 v/\partial x^2+\partial^2 v/\partial y^2 = -\partial \omega/\partial x, \tag{6}$$

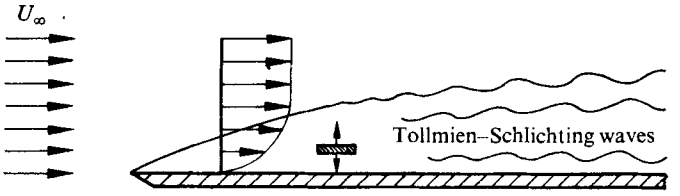

FIGURE 1. Schematic set up of experiments by Schubauer & Skramstad (1948) and Ross *et al.* (1970). Over a flat plate, a ribbon vibrates producing Tollmien–Schlichting waves; the edge of the boundary layer is shown, starting at the leading edge of the plate.

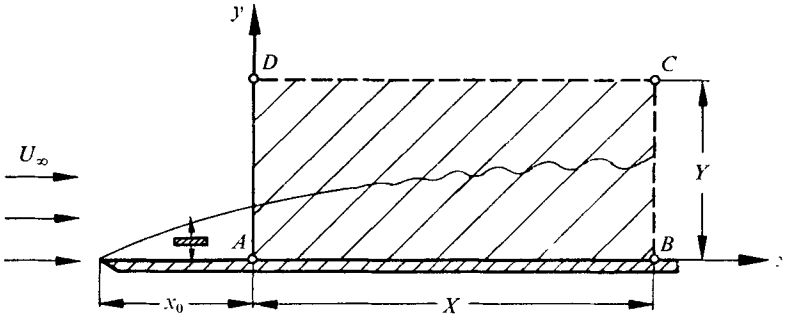

FIGURE 2. Integration domain. The set up is the same as that in figure 1.

which are of Poisson type, are used. They are derived by differentiating (2) with respect to y and x respectively and then using the continuity condition (3). The numerical method is then based on the solution of (1), (5) and (6) in an appropriate integration domain which is specified below.

3. Integration domain

The approach to this investigation and the final concept of the developed numerical method was greatly influenced by the physical set up (figure 1) in the experiments of Schubauer & Skramstad (1948) or Ross *et al.* (1970). In these experiments the established flow over a long flat plate was periodically disturbed by a thin vibrating ribbon within the boundary layer. Then, for small sinusoidal disturbances, the development of Tollmien–Schlichting waves was observed.

For the numerical model the analysis is restricted to the rectangular domain $ABCD$ ($0 \leqslant x \leqslant X$, $0 \leqslant y \leqslant Y$) of figure 2, where the left boundary AD is thought of as being downstream of the vibrating ribbon in the physical experiment. The reaction of the flow to disturbances, which in the numerical model are produced along the left boundary AD, is then determined by the numerical solution of the Navier–Stokes equations within the specified rectangular domain.

To produce the disturbances at the left boundary AD, perturbations obtained from linear stability theory, for example, may be used. Such perturbations are a good approximation of the unsteady flow downstream of the vibrating ribbon in the real experiments. Thus, using such boundary conditions, the numerical

calculations can be considered a numerical simulation of the physical experiments of Schubauer & Skramstad or Ross *et al.*

4. Boundary conditions and initial conditions

One of the major problems of the entire undertaking was the selection of appropriate boundary conditions for the numerical method. The difficulties arise from the complicated nature of the governing equations. For the nonlinear system of partial differential equations (1), (5) and (6), it is not generally possible to decide whether a problem with any given set of boundary conditions is mathematically well posed in the sense of Hadamard (1952). Moreover, it is not at all clear whether Hadamard's postulates for a well-posed problem are adequate for including only physically meaningful solutions. Additional difficulties arise because frequently more boundary conditions are required for finite-difference formulations, i.e. for the numerical solutions, than would be needed for the corresponding differential formulations if exact solutions were possible (Richtmyer & Morton 1967). One is therefore confronted with the task of selecting these extra conditions (which are not known *a priori*) in such a way that the numerical stability of an otherwise stable method is not adversely affected (see also §5). Among several other aspects that also have to be considered in this context one is of special importance. The boundary conditions to be finally adopted have to be such that physically meaningful results can be obtained with a relatively small integration domain to ensure that computational costs are kept within acceptable limits.

Extensive numerical experiments were required to arrive at boundary conditions that are satisfactory with respect to the various considerations discussed previously. The numerical results of §6 demonstrate that the boundary conditions given below are suitable. Especially, the conditions for the downstream boundary BC and the outer boundary CD (figure 2) allow physically meaningful results when the length X of the integration domain is at least four times the disturbance wavelength of the resulting perturbation flow and when the width Y encloses about three boundary-layer thicknesses.

Boundary conditions for the calculation of the unsteady (disturbed) flow

At the wall $y = 0$ the velocity components are zero. For the calculation of the vorticity at the wall a relation is used which can be derived from (6). Thus,

$$u(x,0,t) = v(x,0,t) = 0, \quad \partial\omega(x,0,t)/\partial x = -\partial^2 v(x,0,t)/\partial y^2. \qquad (7)\text{–}(9)$$

At the downstream boundary $x = X$ the following conditions are employed:

$$\partial^2 u'(X,y,t)/\partial x^2 = -\alpha^2 u'(X,y,t), \qquad (10)$$

$$\partial^2 v'(X,y,t)/\partial x^2 = -\alpha^2 v'(X,y,t), \qquad (11)$$

$$\partial^2 \omega'(X,y,t)/\partial x^2 = -\alpha^2 \omega'(X,y,t), \qquad (12)$$

where α is the (real) wavenumber of the resulting perturbation flow (values for α can be obtained from corresponding linear-stability-theory calculations as the

real part of the complex wavenumber for spatial amplification, or determined iteratively as discussed below). The prime denotes the flow variables of the perturbation flow; they are defined as the difference between the total flow variables u, v, ω and the corresponding variables of the undisturbed flow, U, V, Ω:

$$u'(x,y,t) = u(x,y,t) - U(x,y), \quad v'(x,y,t) = v(x,y,t) - V(x,y), \quad (13), (14)$$

$$\omega'(x,y,t) = \omega(x,y,t) - \Omega(x,y). \quad (15)$$

Numerical experiments have shown that (10)–(12) for the downstream boundary were acceptable for the present investigation and were in many ways superior to other versions considered. Their decisive advantage is the relatively small upstream influence, which was thoroughly investigated in numerous test calculations (Fasel 1974). If, for example, $\alpha = 0$ was used as a rather crude assumption for α in (10)–(12), results were never affected more than approximately $\frac{3}{2}$ disturbance wavelengths upstream, whenever the integration domain in the x direction enclosed at least four disturbance wavelengths.

At the upper boundary $y = Y$ zero perturbation vorticity is assumed, while the conditions for the perturbation velocity components imply asymptotic decay in the y direction,

$$\omega'(x, Y, t) = 0, \quad \partial u'(x, Y, t)/\partial y = -\alpha(Re)^{-\frac{1}{2}} u'(x, Y, t), \quad (16), (17)$$

$$\partial v'(x, Y, t)/\partial y = -\alpha(Re)^{-\frac{1}{2}} v'(x, Y, t), \quad (18)$$

where α is again assumed real, as in (10)–(12). Conditions (16)–(18) are consistent with experimental evidence and linear-stability-theory results according to which the perturbation vorticity decays very rapidly in the y direction and is practically zero at about three boundary-layer thicknesses from the wall. The perturbation velocity components, on the other hand, decay rather slowly in the y direction. Using (17) and (18) allows, therefore, a relatively small integration domain in the y direction since it is not necessary to postulate that u' and v' vanish on CD. The boundary conditions (17) and (18) for the outer boundary CD, as well as (10)–(12) for the downstream boundary BC, can be derived assuming neutral periodic behaviour of the perturbation flow near these boundaries. However, the use of these conditions does not force strictly periodic behaviour upon the flow. Rather, test calculations have shown that, with these conditions, damping or amplification of the disturbances is possible even on the boundaries themselves.

Another remark concerning the boundary conditions for boundaries CD and BC is in order at this point. To obtain simple relations on these boundaries one assumes that α is constant, although numerical results, as well as linear stability theory and experiments, indicate that α varies with x. Using a constant value for α in the boundary conditions, however, yields results in which α depends on x, even on the boundaries CD and BC. This property was exploited to determine iteratively $\alpha(x)$, which is then used in the boundary conditions on CD and BC since for practical cases $\alpha(x)$ is not known *a priori*. Even with relatively crude initial guesses for $\alpha(x)$ this iteration loop converges rather rapidly.

At the left boundary $x = 0$ the disturbances are introduced into the numerical

model. Perturbation functions P_u, P_v, P_ω, solely dependent on y and t, are superimposed on the profiles of the undisturbed flow, for which the Blasius solution, denoted by index B, is used:

$$u(0,y,t) = u_B(0,y) + P_u(y,t), \tag{19}$$

$$v(0,y,t) = v_B(0,y) + P_v(y,t), \tag{20}$$

$$\omega(0,y,t) = \omega_B(0,y) + P_\omega(y,t). \tag{21}$$

The perturbation functions, which in this particular study are sinusoidal in time, are discussed in more detail in § 6.

Initial conditions

For initial conditions at $t = 0$ an undisturbed flow field U, V, Ω is assumed throughout the integration domain (disturbances are initiated at $t > 0$),

$$u(x,y,0) = U(x,y), \quad v(x,y,0) = V(x,y), \quad \omega(x,y,0) = \Omega(x,y). \tag{22)–(24}$$

The undisturbed flow field is obtained by first solving the Navier–Stokes equations for the steady flow, i.e. by solving (1), (5) and (6) without the term $\partial\omega/\partial t$ in (1), and using the boundary conditions specified below.

Boundary conditions for the calculation of the steady (undisturbed) flow

At the wall the conditions are equivalent to those of the unsteady flow calculations,

$$U(x,0) = V(x,0) = 0, \quad \partial\Omega(x,0)/\partial x = -\partial^2 V(x,0)/\partial y^2. \tag{25)–(27}$$

The conditions for the downstream boundary are

$$\partial^2 U(X,y)/\partial x^2 = \partial^2 V(X,y)/\partial x^2 = \partial^2 \Omega(X,y)/\partial x^2 = 0. \tag{28)–(30}$$

These conditions are compatible with the downstream boundary conditions (10), (11) and (12) for the unsteady, disturbed flow when disturbances have not yet reached the downstream boundary during the initial, transient stage. Test calculations have verified that indeed no undesirable disturbances are introduced at the downstream boundary during this transient stage when the steady, undisturbed flow is calculated with these conditions.

For the outer boundary the conditions

$$U(x,Y) = 1, \quad \partial V(x,Y)/\partial y = 0, \quad \Omega(x,Y) = 0 \tag{31)–(33}$$

are employed; (32) is derived from the continuity condition (3) taking (31) into account. Finally, for the upstream boundary the profiles of the Blasius solution are used again,

$$U(0,y) = u_B(0,y), \quad V(0,y) = v_B(0,y), \quad \Omega(0,y) = \omega_B(0,y). \tag{34)–(36}$$

The argument could be raised that instead of using as initial conditions the solution of the steady Navier–Stokes equations with Blasius profiles at the upstream boundary one could use with equal justification the Blasius solution itself in the

entire flow field. Indeed, the numerical solution of the Navier–Stokes equations for the steady flow yields results that closely agree with the Blasius solution, so that plotted profiles practically coincide. In this study, however, the reaction of the flow to very small disturbances is being investigated and therefore the use of the Blasius solution could initially cause disturbances of the same order of magnitude as the forced perturbations and thus distort the transient character of the flow. Using the solution of the Navier–Stokes equations any such undesirable initial distortion of the transient flow is avoided.

5. Numerical solution

The problem posed requires first the solution of a boundary-value problem for the calculation of the steady flow, i.e. solution of (1), (5) and (6) (without $\partial\omega/\partial t$ in (1)) with boundary conditions (25)–(36). Second, the solution of a mixed initial-boundary-value problem for the calculation of the unsteady flow is required, i.e. solution of (1), (5) and (6) with boundary conditions (7)–(21) and initial conditions (22)–(24). The partial differential equations are in both cases of sixth order, in contrast to the fourth order of the more customary ω, ψ formulation used in most numerical solutions of the Navier–Stokes equations. The partial differential equations are of elliptic type with regard to the space co-ordinates, that is, for the calculation of the steady flow, and of parabolic type for the calculation of the unsteady flow.

For the numerical solution of the problem posed, a finite-difference method was developed. Such a difference method for the intended investigation of stability and transition of boundary-layer flows has to meet a number of requirements in order to ensure success. Some of the requirements deemed most important in this context are discussed below.

(i) *Stability, convergence.* Rigorous mathematical proofs of (numerical) stability and convergence for nonlinear problems as difficult as the one at hand have not been accomplished as yet. For the present investigation, however, stability of the numerical method is of fundamental importance. Numerical instability is frequently exhibited in the form of oscillations which would be hardly discernible from the physically meaningful oscillations caused by the introduced forced perturbations. Hence, strong emphasis had to be placed on the development of an extremely stable finite-difference method, even for relatively large Reynolds numbers, since to see physical instability and the amplification of disturbances it is necessary to experiment with Reynolds numbers larger than the critical Reynolds number.

For this particular study, the problem of convergence is not quite as serious. However, convergence is not necessarily guaranteed if for a properly posed problem the numerical scheme is stable and consistent as is the case for linear partial differential equations of second order.† By experimenting with small periodic disturbances one can check empirically the convergence behaviour of the numerical method by comparing calculations for various grid sizes with linear-stability-theory results and experimental measurements.

† Lax's equivalence theorem; see Richtmyer & Morton (1967).

(ii) *Accuracy of second order.* For this investigation at least second-order accuracy of the numerical method (i.e. the truncation error of the difference analogue to the governing equations, initial and boundary conditions at least of second order) is required to exclude or minimize undesirable non-physical effects, such as artificial viscosity, when mesh intervals of practical sizes are used. Numerical experiments by Cheng (1970) with a simpler model equation have shown that an accuracy of at least second order is necessary when solutions are of a periodic nature.

(iii) *Realistic resolution of the transient character of unsteady flow fields.* The flow under investigation is of extremely unsteady nature, with the time-dependent behaviour of the flow being of special interest. Thus, the difference method has to be such that a realistic resolution of the transient character of such flow fields is possible in order to enable investigation of unstable perturbation waves. Many popular time-dependent methods, although based on the complete Navier–Stokes equations for unsteady flows, are not applicable because the transient character cannot be properly resolved. Results are therefore only valid when a steady state is reached.

(iv) *Efficiency with respect to computational speed and required storage capacity.* Numerical solutions of the complete Navier–Stokes equations for the type of flows investigated here require numerous time-consuming numerical operations and therefore computers with large, fast-access computer storage capacity, reaching the limits of even modern computer systems, are necessary. A prospective difference method for such an investigation has to be extremely efficient, i.e. maximizing computational speed and minimizing required computer storage capacity as far as possible, in order to be capable at all of undertaking an investigation of this nature with the computers available today.

Of the requirements discussed here, numerical stability is the most stringent one and hence has to be given most consideration. For this reason an implicit method was chosen. Implicit methods are generally much more stable than their explicit counterparts. However, in respect of requirement (iv) preference should have been given to explicit methods because they generally demand less fast-access computer storage capacity and less numerical and programming skills for achieving high computational speed. So, to satisfy requirement (iv) much effort had to be dedicated to developing an extremely efficient implicit difference method that also met the other requirements discussed previously.

Implicit finite-difference method

Experimentation with various implicit difference schemes suggested that a 'fully' implicit scheme with three time-levels was the most promising for this investigation. In this context, 'fully' implicit means that all difference approximations and nodal values for the approximation of governing equations and boundary conditions are taken at the most recent time-level, denoted by integer l (see figures 3 and 4). A three-level method is employed to obtain a truncation error of second order for the time derivative $\partial\omega/\partial t$ in (1). For all space derivatives central differences with second-order truncation error are used.

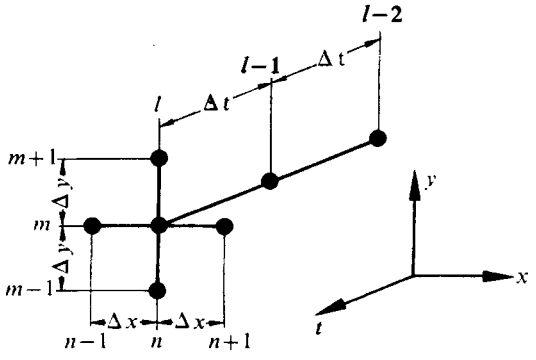

FIGURE 3. Difference molecule.

The fully implicit difference scheme leads to three systems of nonlinear algebraic equations for the calculation of the unknown grid variables. Therefore, the development of efficient algorithms for the solution of very large, nonlinear systems of equations was a matter of great importance. For the solution of the difference-equation systems a line-iteration method was finally adopted with simultaneous iteration of all three equation systems. The line iteration is organized such that nodal values on grid lines parallel to the y axis are determined by a direct method† while proceeding iteratively in the x direction. An important advantage that greatly improved the overall efficiency of the method resulted from combining the two iteration loops, the first required because of the line iteration and the second because of the nonlinear terms, into a single iteration loop.

With this iteration loop the difference equations can be written (i is the iteration index)

$$(\Delta y^2/2\Delta t)\,(t_1\,\omega^{l,i}_{n,m}-t_2\,\omega^{l-1}_{n,m}+t_3\,\omega^{l-2}_{n,m})+(\Delta y^2/2\Delta x)\,u^{l,i-1}_{n,m}(\omega^{l,i-1}_{n+1,m}+2\omega^{l,i}_{n,m}-2\omega^{l,i-1}_{n,m}$$
$$-\omega^{l,i}_{n-1,m})+\tfrac{1}{2}\Delta y\,v^{l,i-1}_{n,m}(\omega^{l,i}_{n,m+1}-\omega^{l,i}_{n,m-1})-(Re)^{-1}(\Delta y/\Delta x)^2\,(\omega^{l,i-1}_{n+1,m}-2\omega^{l,i}_{n,m}+\omega^{l,i}_{n-1,m})$$
$$-\omega^{l,i}_{n,m+1}+2\omega^{l,i}_{n,m}-\omega^{l,i}_{n,m-1}=0, \qquad (37)$$

$$(Re)^{-1}(\Delta y/\Delta x)^2\,(u^{l,i-1}_{n+1,m}-2u^{l,i}_{n,m}+u^{l,i}_{n-1,m})+u^{l,i}_{n,m+1}-2u^{l,i}_{n,m}+u^{l,i}_{n,m-1}$$
$$-\tfrac{1}{2}\Delta y(\omega^{l,i}_{n,m+1}-\omega^{l,i}_{n,m-1})=0, \qquad (38)$$

$$(Re)^{-1}(\Delta y/\Delta x)^2\,(v^{l,i-1}_{n+1,m}-2v^{l,i}_{n,m}+v^{l,i}_{n-1,m})+v^{l,i}_{n,m+1}-2v^{l,i}_{n,m}+v^{l,i}_{n,m-1}$$
$$+(\Delta y^2/2\Delta x)\,(\omega^{l,i-1}_{n+1,m}+2\omega^{l,i}_{n,m}-2\omega^{l,i-1}_{n,m}-\omega^{l,i}_{n-1,m})=0, \qquad (39)$$

where $1 \leqslant n \leqslant N-1, \quad 1 \leqslant m \leqslant M-1, \quad l = 0, 1, 2, \ldots,$

and
$$t_1 = t_2 = t_3 = 0 \quad \text{for} \quad l = 0 \quad \text{(steady flow)},$$
$$\left.\begin{aligned} t_1 = t_2 = 2, \quad t_3 = 0 \quad &\text{for} \quad l = 1 \\ t_1 = 3, \quad t_2 = 4, \quad t_3 = 1 \quad &\text{for} \quad l > 1 \end{aligned}\right\} \quad \text{(unsteady flow)}.$$

The term $2\omega^{l,i}_{n,m}-2\omega^{l,i-1}_{n,m}$ in (37) and (39) has nothing to do with the difference approximation as such; the two parts cancel when the iteration has converged and are only added to improve the convergence characteristics of the iteration loop, especially for high Reynolds numbers. Further considerable improvement

† Algorithm by Thomas (1949) for tri-diagonal coefficient matrices, modified to include simultaneous calculation of vorticity at the wall.

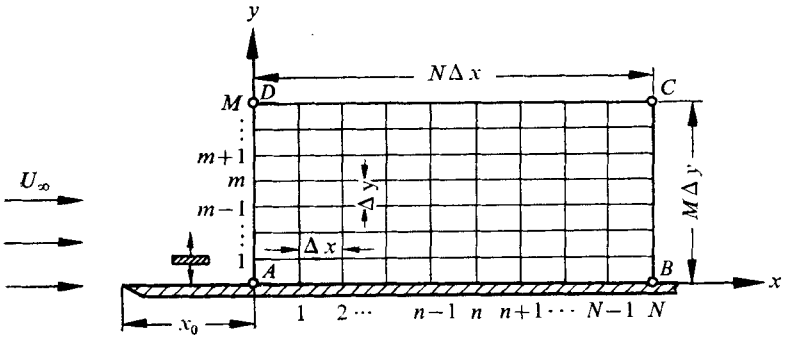

FIGURE 4. Grid arrangement in the x, y plane. Comparing with figure 2, we see that $X = N\Delta x$ and $Y = M\Delta y$.

of the convergence behaviour was achieved by coupling equation systems (37) and (39) through the use of (9) taking $\partial^2 v/\partial y^2$ at iteration level i. Details of the numerical method are discussed elsewhere (Fasel 1974).

6. Numerical results for periodic disturbances of small amplitudes

Test calculations for an unstable and a stable boundary-layer flow

The numerical method was thoroughly checked on a number of relatively small test cases, two of which are discussed here in more detail. They are shown on a stability diagram of linear stability theory (figure 5) obtained from numerical solution of the Orr–Sommerfeld equation for the case of spatial disturbance amplification (Wazzan *et al.* 1968; Jordinson 1970).

In the chosen representation of figure 5, dimensionless disturbance frequency $\beta^* = \bar{\beta}\delta_1/U_\infty$ versus Reynolds number $Re^* = U_\infty \delta_1/\nu$ (δ_1 displacement thickness), the dimensional disturbance frequency $\bar{\beta}$ or a dimensionless frequency parameter $F = 10^4\bar{\beta}\nu/U_\infty^2$ is constant on rays through the origin. Thus, the perturbation conditions of the flow downstream of a constant frequency disturbance correspond to points on a ray through the origin. Proceeding from the disturbance location in the downstream direction corresponds to moving away from the origin. Disturbances should therefore become amplified at downstream locations corresponding to points within the unstable region (inside the neutral stability curve) and damped at locations corresponding to points in the stable region (outside the neutral stability curve).

The two test cases discussed here are both on the ray $F = 1{\cdot}316$ shown in figure 5. For test case 1 the location of the left boundary AD of the rectangular integration domain corresponds to a point on the lower branch of the neutral stability curve at $Re^* = 635$. When proceeding in the downstream direction the unstable region is entered and distrubances should therefore grow. For test case 2 the calculation starts at $Re^* = 970$, a point inside the unstable region, a short distance from the upper branch of the neutral stability curve. Therefore, the disturbances should first grow and then decay after the neutral stability curve is crossed.

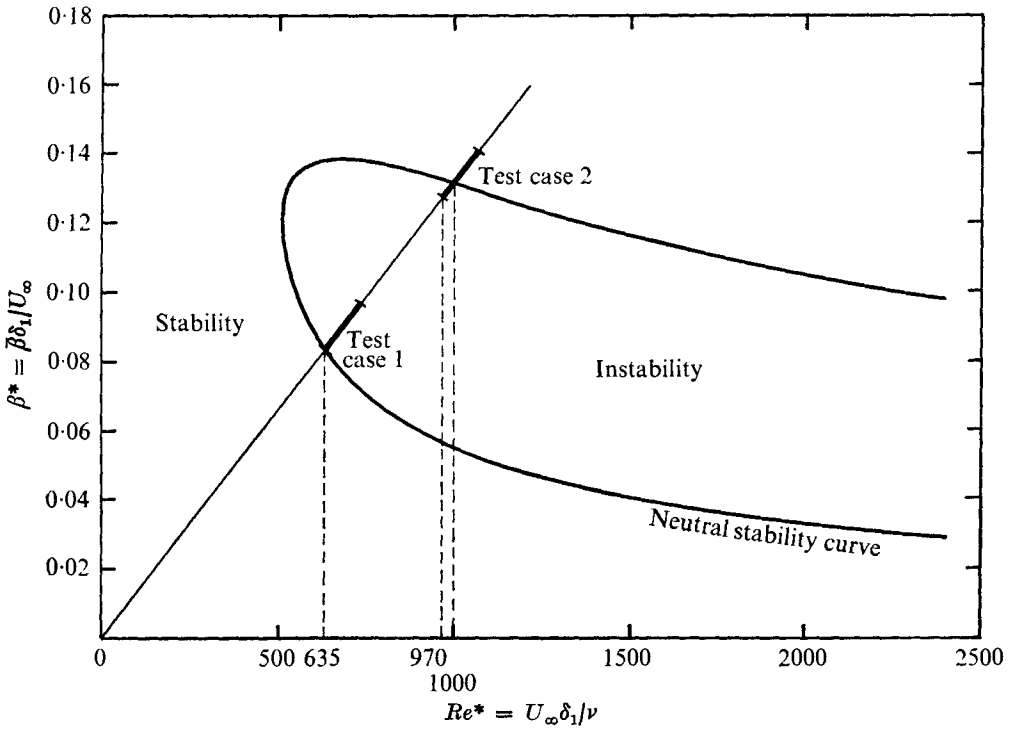

FIGURE 5. Two test cases on the stability diagram of linear stability theory. On the straight line, $\bar{\beta}$ and F are constant (see text); in this case $F = 1{\cdot}316$.

For periodic (sinusoidal in time) disturbances the perturbation functions in the upstream boundary conditions (19)–(21) can be written

$$P_u(y,t) = \hat{a}u_A'(y)\cos(\beta t), \tag{40}$$

$$P_v(y,t) = \hat{a}v_A'(y)\cos(\beta t + \tfrac{1}{2}\pi), \tag{41}$$

$$P_\omega(y,t) = \hat{a}\omega_A'(y)\cos(\beta t). \tag{42}$$

For the present calculations the common amplitude factor $\hat{a}$ was selected so that the absolute maximum value of P_u was 0·05 % of the free-stream velocity. The so-called amplitude distributions or perturbation profiles $u_A'(y), v_A'(y), \omega_A'(y)$ were taken from numerical solutions of the Orr–Sommerfeld equation for spatial amplification (Jordinson 1970, Kümmerer 1973).

The perturbation profiles used in test case 1, for example, are shown in figure 6(*a*), together with the corresponding phase relations of linear stability theory in figure 6(*b*) (solid curves). However, when using the simple cosine relations in (40)–(42) the phase relations are approximated by the straight (dashed) lines. The phase change in the u' and ω' perturbations near the wall is taken into account in a relatively crude manner by using the dashed curves for the perturbation profiles u_A' and ω_A' in figure 6(*a*). With these perturbation functions any y variation in the phase relation is completely neglected. The phase difference of approximately $\frac{1}{2}\pi$ between the u' and v', as well as the ω' and v', perturbations is consistent with linear stability theory and is represented in (40)–(42).

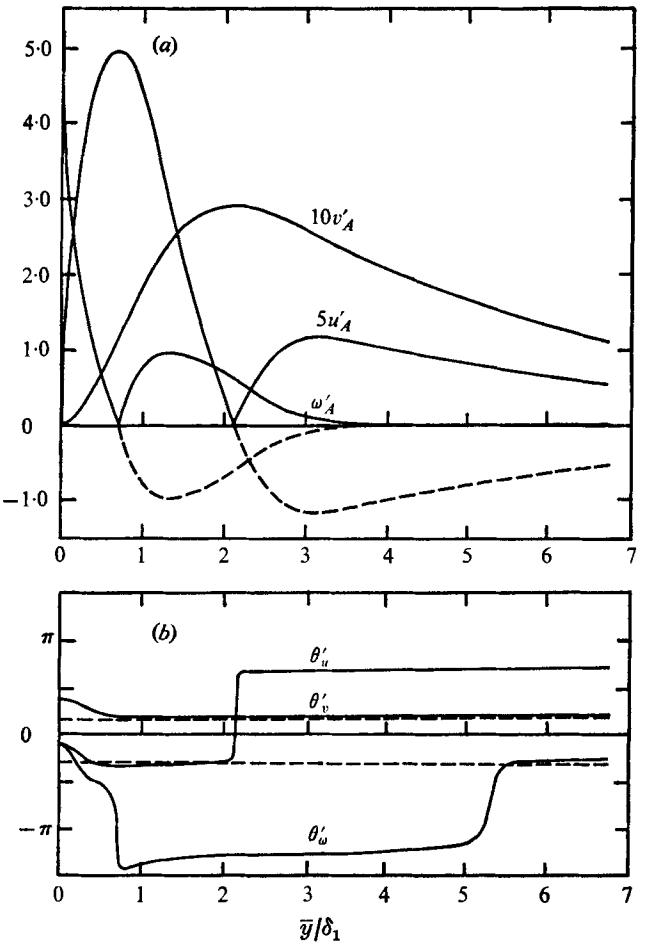

FIGURE 6. (*a*) Perturbation profiles (amplitude distributions) and (*b*) phase relations of linear stability theory for $F = 1{\cdot}316$, $Re^* = 635$.

	Test case		Calculation				
	1	2	A (step 1)	A (step 2)	B	C	D
Δx	0·017	0·017	0·017	0·017	0·014	0·012	0·010
Δy	0·283	0·432	0·260	0·442	0·234	0·208	0·208
Δt	0·025	0·025	0·025	0·025	0·020	0·015	0·013

TABLE 1. Grid intervals

For these calculations the grid parameters were selected as follows: in the x direction, 40 intervals were used with Δx chosen as approximately $\frac{1}{10}$ of the disturbance wavelength; in the y direction, 48 intervals were used with Y approximately 3 boundary-layer thicknesses. The time increment Δt was chosen as approximately $\frac{1}{20}$ of a time period. The values of the grid intervals used in the calculations discussed in this paper are given in table 1. These interval sizes were

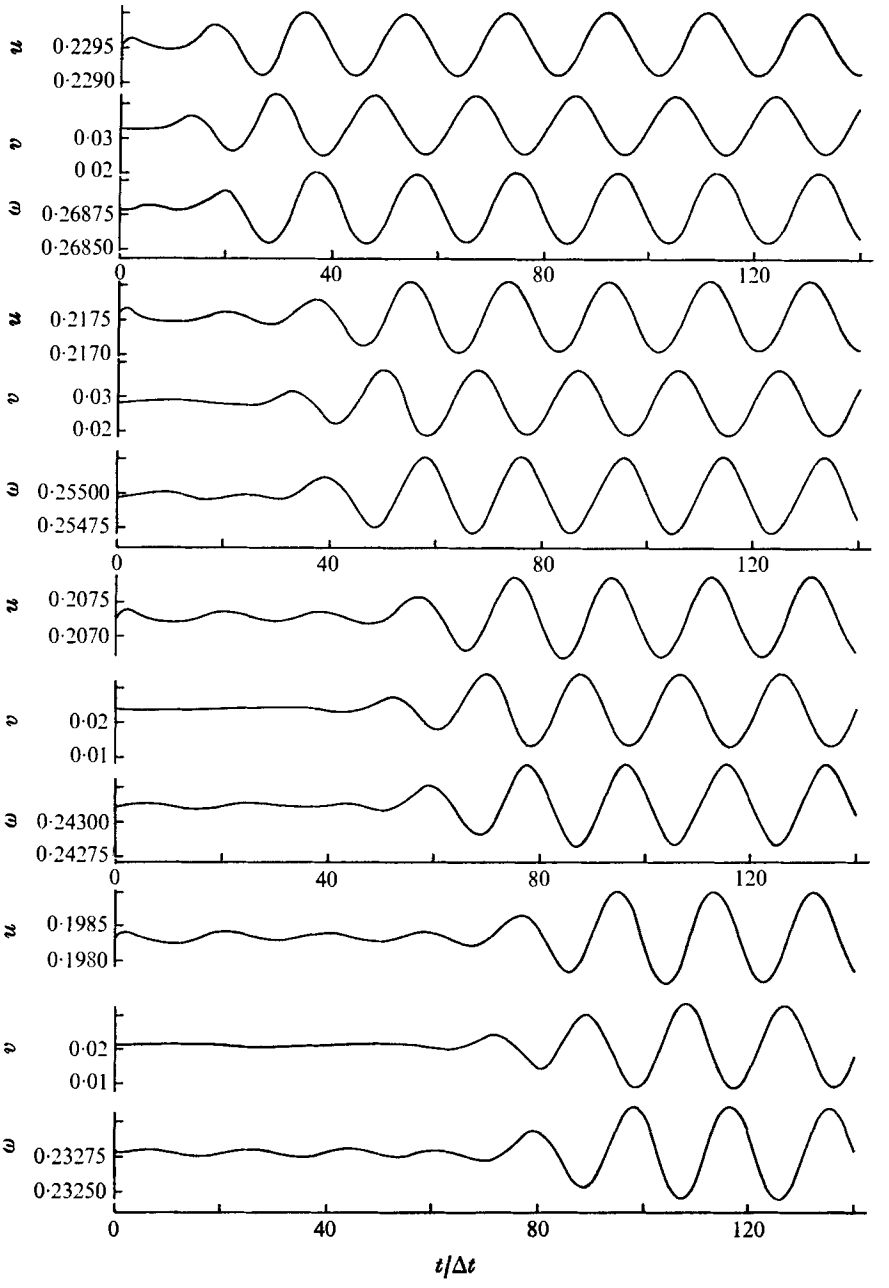

FIGURE 7 (*a*). For legend see opposite page.

adopted after extensive numerical experiments had been conducted to investigate the convergence behaviour (accuracy) of the method (Fasel 1974). For this purpose selected test cases were recalculated with smaller and smaller interval sizes. The interval sizes finally used for the calculations discussed in this paper were sufficiently small to warrant accurate enough results for reasonable compari-

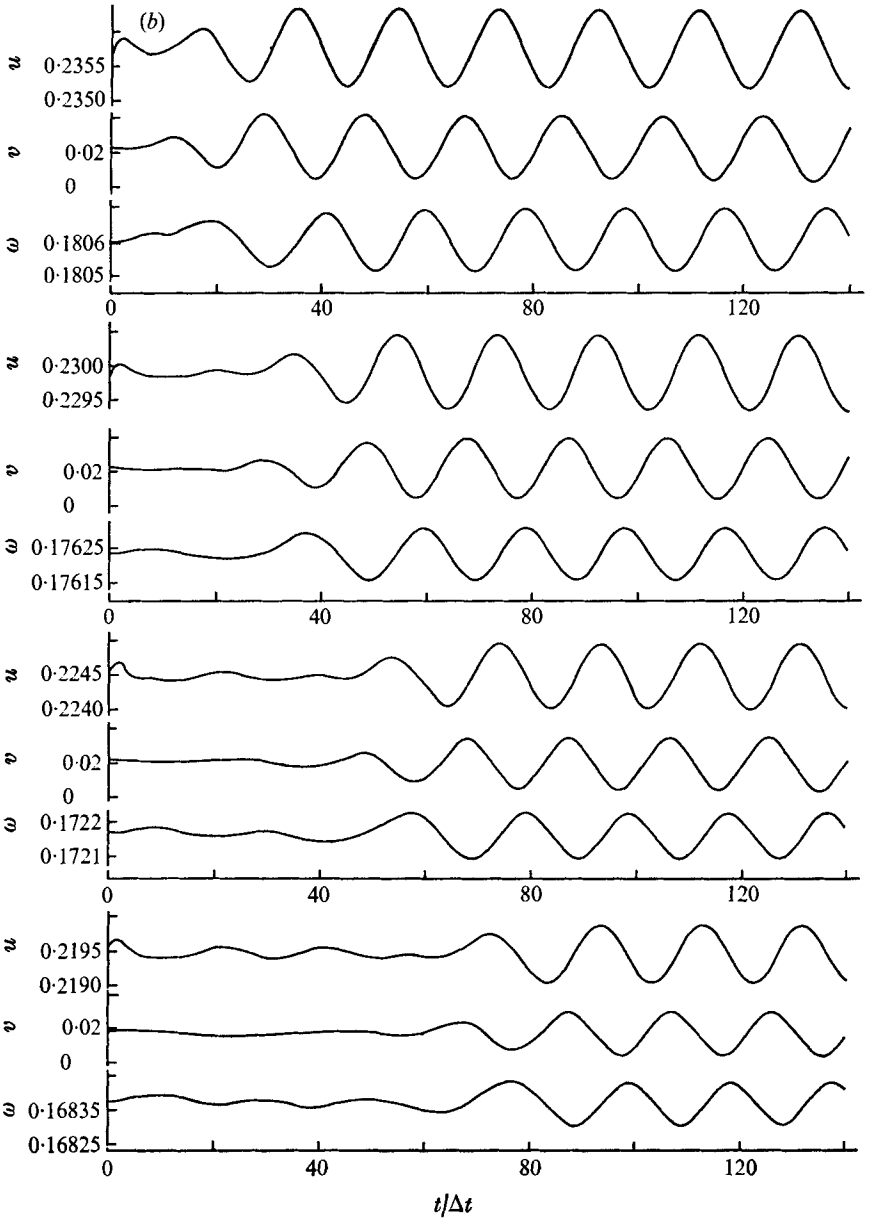

FIGURE 7. Temporal development of periodically disturbed flow for (*a*) test case 1, (*b*) test case 2 at $y/\Delta y = 3$ and four different downstream locations, reading from top to bottom, $x/\Delta x = 8, 18, 28, 38$.

son with experimental measurements and linear stability theory while keeping computational costs within acceptable limits. For example, calculations with the above interval sizes sliced in half lead to maximum relative deviations in the computed perturbation variables always less than 1% for any location within the integration domain.

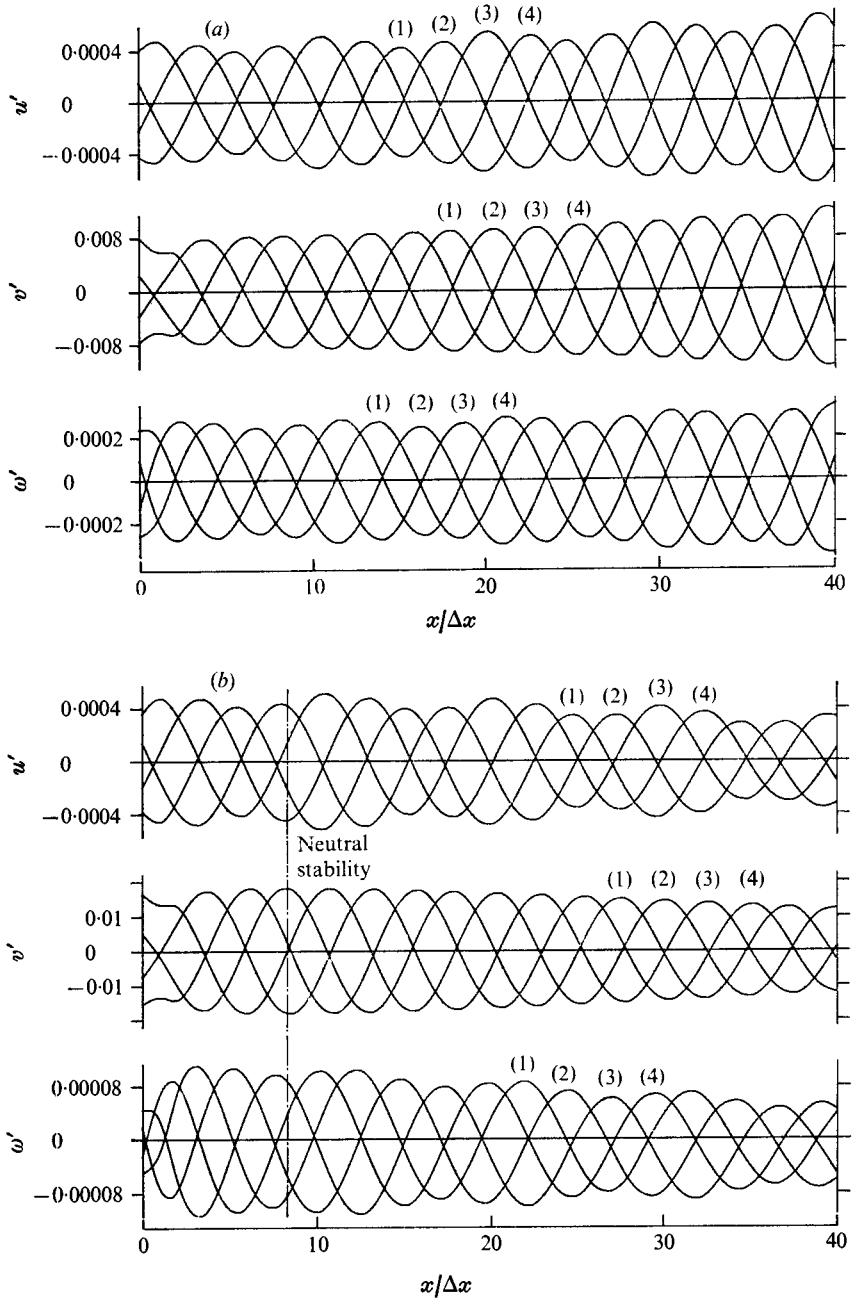

FIGURE 8. Downstream development of perturbations at $y/\Delta y = 3$ for four different time levels. (*a*) Test case 1, (*b*) test case 2. The time levels are (1) $t/\Delta t = 125$, (2) $t/\Delta t = 130$, (3) $t/\Delta t = 135$, (4) $t/\Delta t = 140$.

For rigorous quantitative comparison with linear stability theory, calculations with greater accuracy, i.e. smaller interval sizes, would be desirable, requiring, of course, much larger computation times. However, this paper does not intend to compete in accuracy with linear-stability-theory calculations, something which could only be done at excessive computational cost; it intends rather to demonstrate the suitability of the developed numerical method for stability studies.

Typical numerical results for the two test cases are shown in figures 7–10. An impression of the temporal development of the disturbed flow and of the propagation of the time-wise sinusoidal disturbances which are introduced at the upstream boundary can be obtained from figure 7. The flow variables u, v, ω are plotted for a constant distance $y/\Delta y = 3$ versus time $t/\Delta t$ at four different downstream x stations, at 8, 18, 28 and 38 $x/\Delta x$ from the upstream boundary AD. After some time has elapsed the flow behaviour is obviously of a periodic nature which is first reached near the upstream boundary and last near the downstream boundary. This is reasonable since the introduced sinusoidal disturbances should propagate downstream with the finite velocity β/α. For test case 1 in figure 7 (a) the amplitudes of the periodic oscillations increase in the downstream direction (the scale is the same for all x stations) while for test case 2 in figure 7 (b) the amplitudes decrease.

The downstream development of the flow is elucidated more clearly in figure 8, where the perturbation variables u', v', ω' are plotted against the downstream co-ordinate $x/\Delta x$ for the same constant distance $y/\Delta y = 3$ from the wall. In every diagram four different curves are plotted, each corresponding to a different time level. At these time levels the flow has already reached a time-wise periodic behaviour in the entire flow field, i.e. a quasi-steady state exists. As predicted by linear stability theory the curves for test case 1 in figure 8 (a) clearly exhibit amplification of the disturbances in the downstream direction. For test case 2 in figure 8 (b) first an amplification of the disturbances can be observed followed by damping when the neutral curve is crossed. For the u' and ω' perturbations the growth or decay of amplitudes is wave-like, contrary to the v' perturbations. This matter will be brought up again later.

A survey of the perturbation flow behaviour in the entire integration domain is portrayed in figure 9. There, the perturbation profiles (amplitude distributions) of the u', v' and ω' perturbations are plotted at every other consecutive x station, starting at the left boundary $x/\Delta x = 0$ and ending at the right boundary $x/\Delta x = 40$. For a given x station these profiles are obtained by determining at every discrete y location the maximum absolute value of the perturbation variables over an entire time period. The shapes of the calculated perturbation profiles qualitatively resemble those of linear stability theory, with the typical phase reversals near the wall for the u' and ω' perturbations also being present (the profiles plotted at $x/\Delta x = 0$ actually are from linear stability theory; they are used to disturb the flow). Following the development of the amplitudes in the downstream direction for a constant distance $y/\Delta y$ from the wall, in figure 9 (a) for test case 1 a growth of amplitudes can be observed again while for test case 2 in figure 9 (b) the amplitudes decrease. (The irregular growth or decay behaviour of the u' and ω' perturbations is noticeable again.) In figure 9 the

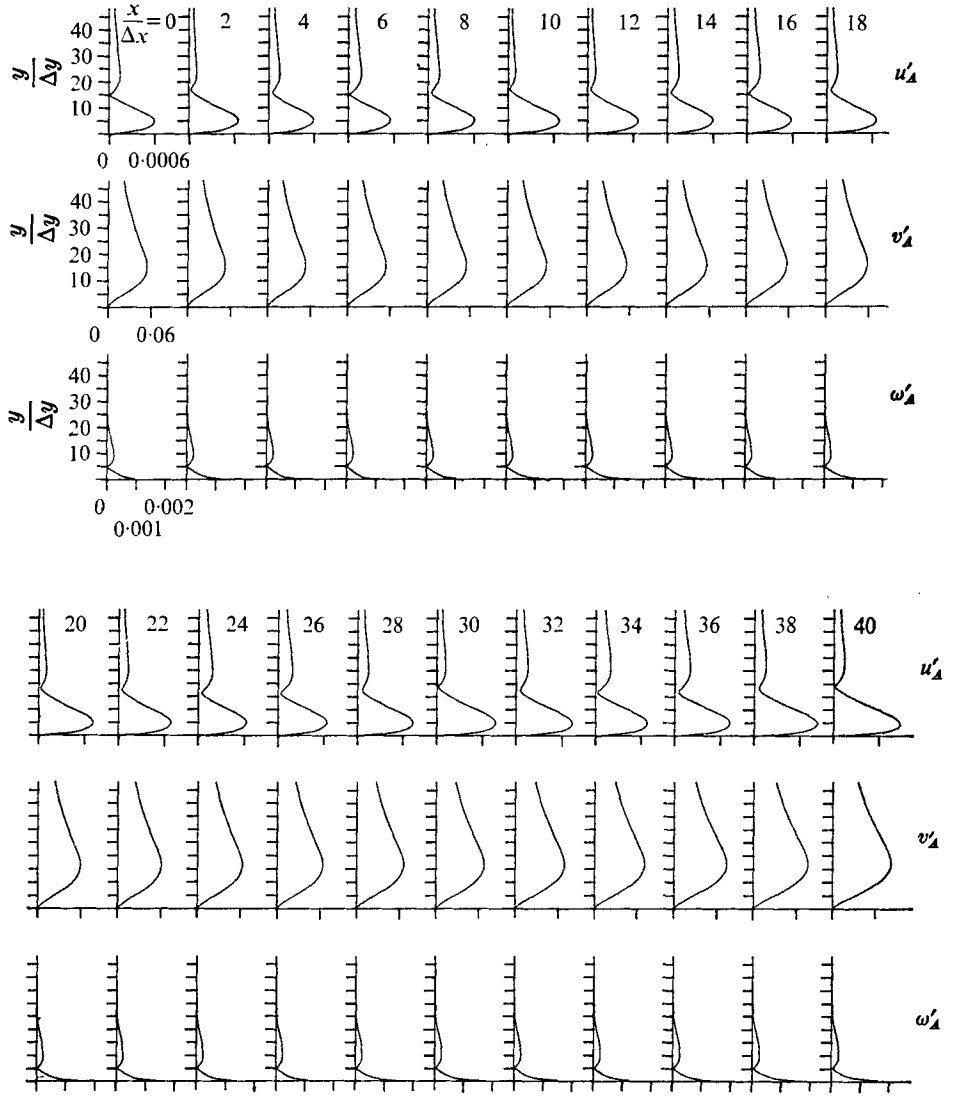

FIGURE 9 (*a*). For legend see opposite page.

downstream development of the maximum values of the perturbation profiles is of special interest: for the ω' perturbations they are at the wall, for the u' perturbations they are close to the wall and for the v' perturbations further away.

In figure 10 these maximum values (made dimensionless with the corresponding values at $x/\Delta x = 0$) are plotted against x. The aforementioned wavy behaviour of the u'_A and ω'_A perturbation amplitudes is now clearly observable. The v'_A perturbations, however, do not show such behaviour. For better comparison of the amplification rates the median curves of the u'_A and ω'_A perturbation amplitudes are also plotted in figure 10. Additional investigations indicated that the wavy character is caused by the relatively crude phase relationships in the per-

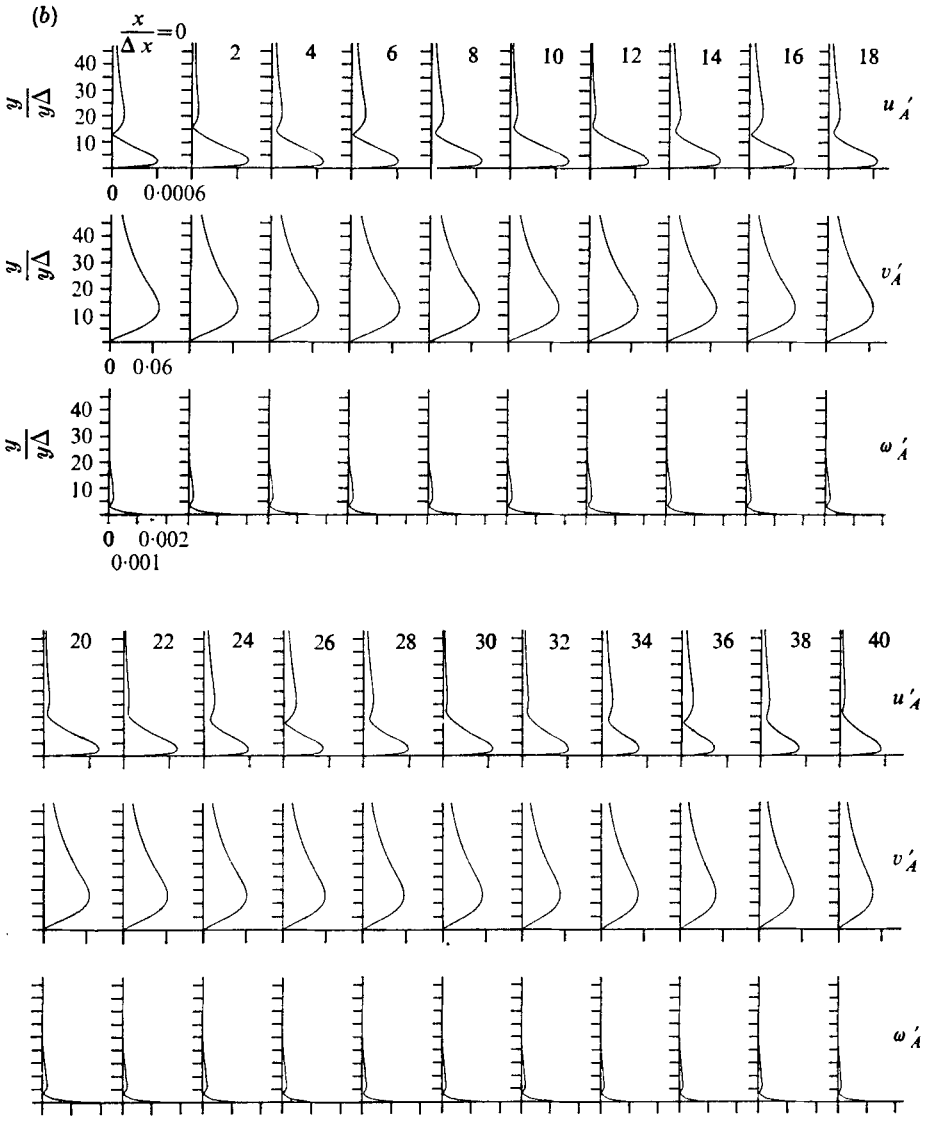

FIGURE 9. Perturbation profiles (amplitude distributions) at every other consecutive downstream location. (*a*) Test case 1, (*b*) test case 2.

turbation functions (40)–(42). When using, for example, phase relationships as obtained from linear stability theory, the numerical calculations yield results for which such behaviour is virtually absent. This context can be explained as follows: when using the phase relationships of linear stability theory, the condition

$$\int_0^\infty u'dy = 0$$

is always satisfied during the entire time period of the sinusoidal cycle. However, with the crude phase relationships used for the calculations here, this condition is

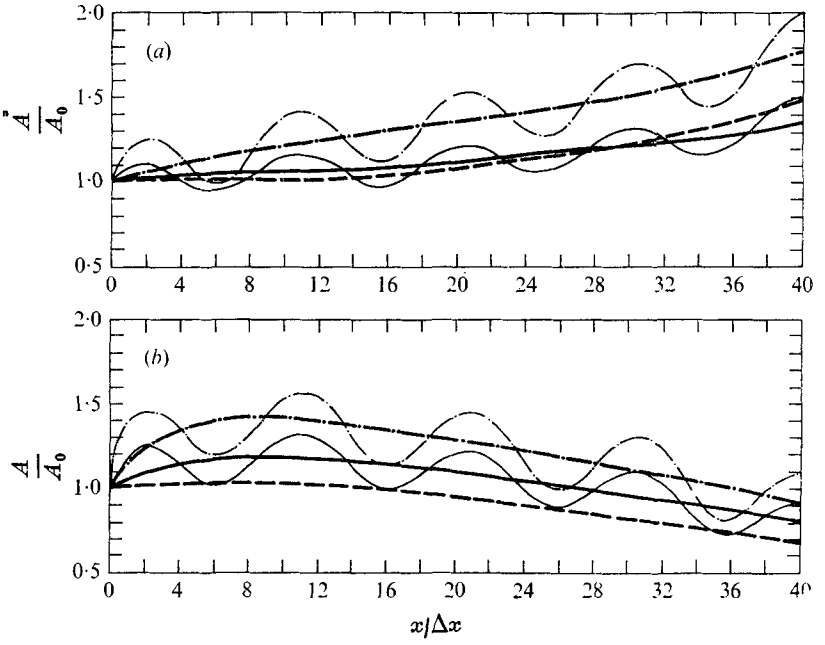

FIGURE 10. Downstream development of maximum perturbation amplitudes. (*a*) Test case 1, (*b*) test case 2. ——, $(u_A')_{\max}/[(u_A')_{\max}]_{x=0}$; - - -, $(v_A')_{\max}/[(v_A')_{\max}]_{x=0}$; —·—·—, $(\omega_A')_{\max}/[(\omega_A')_{\max}]_{x=0}$. The slowly varying curves —— and —·—·— are median curves.

violated. This causes an additional oscillatory mode with the same frequency (as the primary disturbance wave) which is superimposed on the basic Blasius flow. Thus these calculations, strictly speaking, can be considered as a stability investigation of a slightly oscillating boundary-layer flow with identical frequencies to the oscillating basic flow and the generated sinusoidal disturbances. It should be mentioned, however, that the amplitudes of the resulting oscillatory modes in the basic flow are so small that the amplification rates (median curves in figure 10) are not affected when phase relationships of linear stability theory are used, i.e. when the oscillatory mode of the basic flow is avoided.

The amplification curves in figure 10 clearly show for test case 1 (figure 10*a*) the predicted growth of the disturbance amplitudes while for test case 2 (figure 10*b*) the disturbance amplitudes at first grow and then decrease after the neutral stability curve is crossed. It can also be observed that the growth rates for the u', v' and ω' perturbations differ from one another. In fact, amplification curves for different constant distances from the wall would all be different. This phenomenon is in contrast to classical linear stability theory, where for the case of space-wise amplification the amplification rate is independent of the wall distance. However, these findings are in agreement with experimental evidence (Ross *et al.* 1970; see also Jordinson 1968) and more recent stability investigations (Bouthier 1972, 1973; Gaster 1974).

The results for the two test cases discussed here, as well as for a number of other calculations of a similar nature, have demonstrated at least qualitative agreement

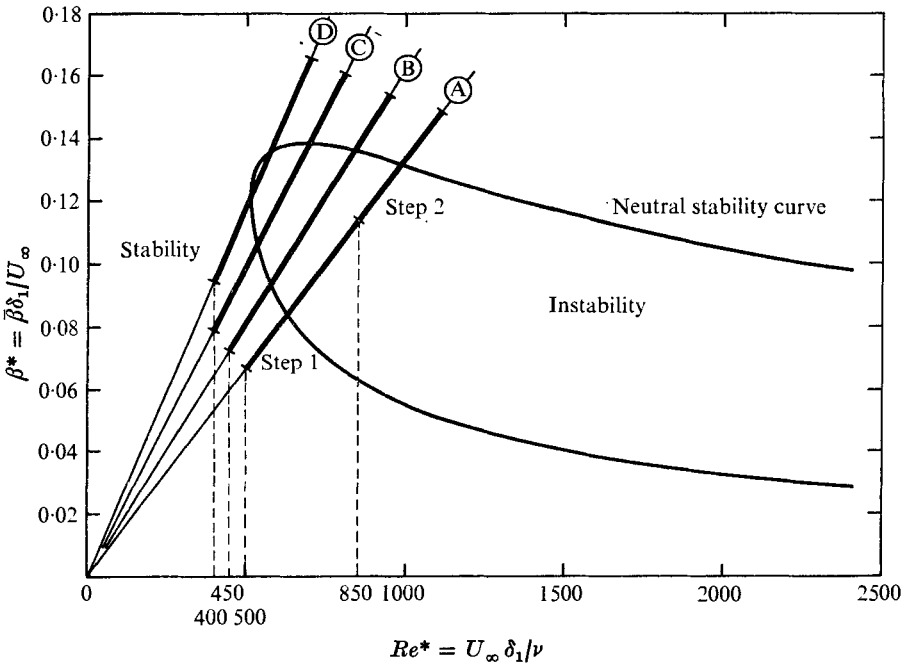

FIGURE 11. Calculations A, B, C, D on stability diagram of linear stability theory. The values of F which correspond to the calculations are (A) 1·316, (B) 1·6, (C) 2·0 and (D) 2·4.

with linear stability theory: disturbances were amplified in the unstable region and damped in the stable region of linear stability theory.

Comparison of numerical results with linear stability theory and experiments

For a more quantitative comparison with linear stability theory and experimental measurements, calculations were made for which the entire region of instability is traversed on rays F = constant as shown in figure 11. The calculations start in the stable region and, after traversing the unstable region inside the neutral curve, end again in the stable region. Calculation A with $F = 1{\cdot}316$ consists of two steps: the first step from $Re^* = 500$ to $Re^* = 850$ and the second step from $Re^* = 850$ to $Re^* = 1100$. For calculations B, C and D the region of instability is traversed in a single step. (For values of the grid intervals used in these calculations see table 1.)

For the two-step calculation the perturbation variables u', v', ω' are plotted in figure 12 against $x/\Delta x$. The perturbation variable v' for calculations B, C and D is shown in figure 13 against $x/\Delta x$. As before, there are four curves in each diagram corresponding to four different time-levels after the quasi-steady state was established. The curves in figure 12(*a*) for step 1 of calculation A first exhibit decay of the disturbance amplitudes until the lower branch of the neutral stability curve is reached whereupon the amplitudes increase. In figure 12(*b*) for step 2 the disturbances continue to grow in the downstream direction until they reach the location of the upper branch of the neutral curve and are damped from

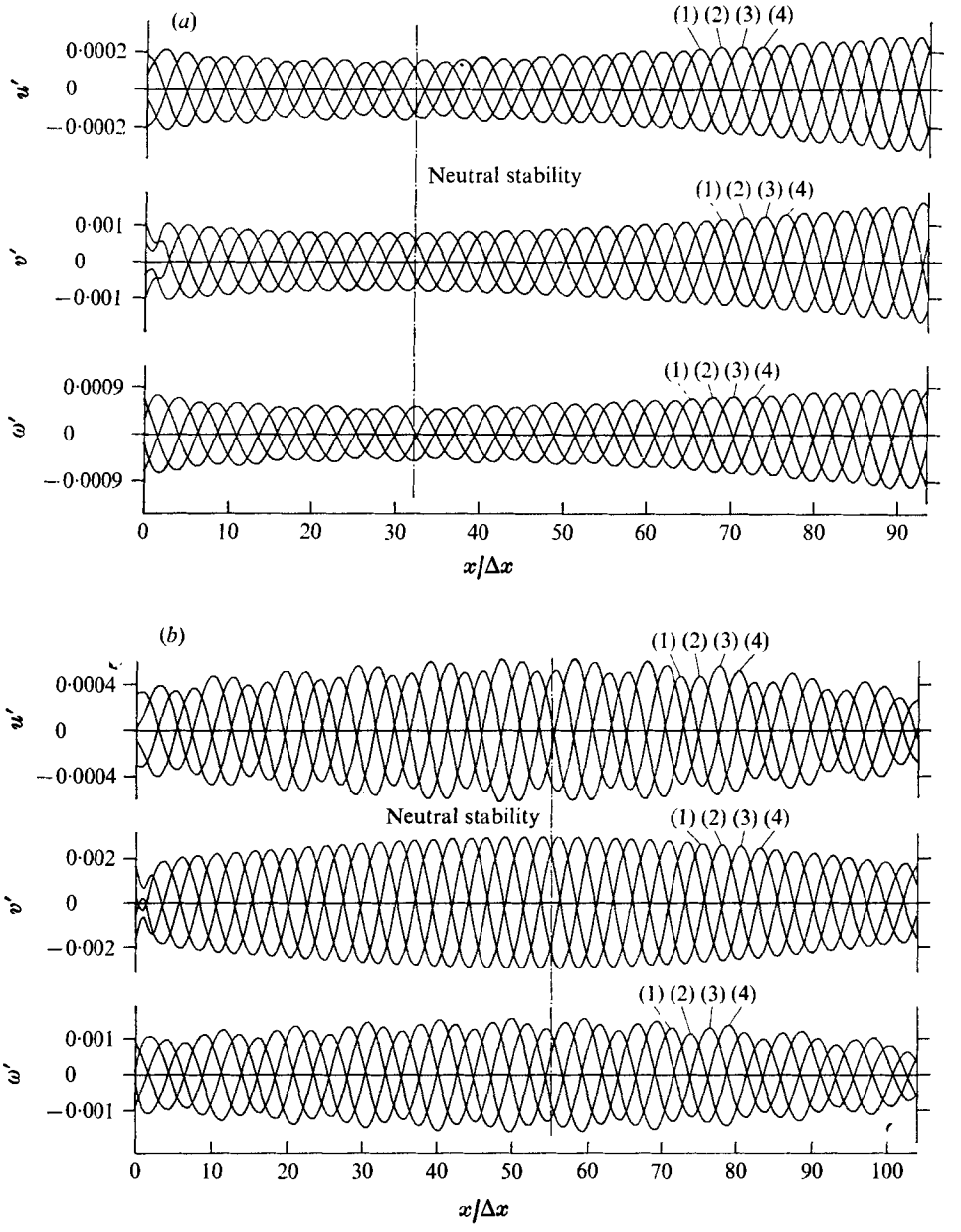

FIGURE 12. Downstream development of perturbations at $y/\Delta y = 3$ for four different time levels. Calculation A, (*a*) step 1, the values of $t/\Delta t$ are (1) 285, (2) 290, (3) 295, (4) 300; (*b*) step 2, the values of $t/\Delta t$ are (1) 295, (2) 300, (3) 305, (4) 310.

there on. In figure 13 for calculations B, C and D, for which the unstable region is traversed in a single step, it is possible to observe damping of the disturbances in the stable region, amplification in the unstable region and again damping in the stable region. With increasing disturbance frequencies (frequencies increase from A to D) the transition from damping to amplification at the lower branch

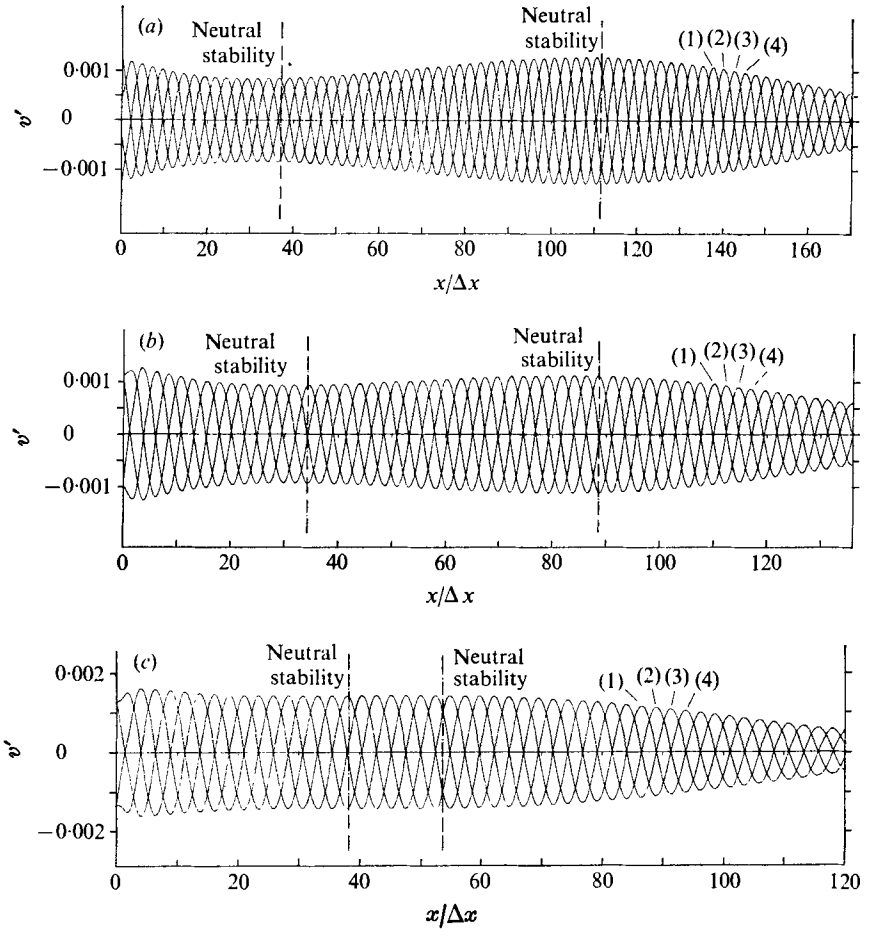

FIGURE 13. Downstream development of v' perturbations at $y/\Delta y = 3$ for four different time levels. (*a*) Calculation B, the values of $t/\Delta t$ are (1) 485, (2) 490, (3) 495, (4) 500; (*b*) calculation C, $t/\Delta t$ = (1) 385, (2) 390, (3) 395, (4) 400; (*c*) calculation D, $t/\Delta t$ = (1) 355, (2) 360, (3) 365, (4) 370.

of the neutral stability curve becomes less and less pronounced; for calculation D any such transition is hardly noticeable at all.

In figure 14 the amplification curve, which is obtained from the inner maximum of the u' perturbation profiles for calculation A, is compared with appropriate experimental points by Ross *et al.* (1970) (see also Jordinson 1968; Barnes 1966). Direct comparison with the experimental points (which are from root-mean-square value measurements from the inner maximum of the u' perturbations) is admissible since in both cases the amplitude values are normalized by their respective minima. Additionally, in figure 14 two amplification curves of linear stability theory are shown for comparison, one obtained from a numerical solution of the Orr–Sommerfeld equation (Jordinson 1968, 1970; Kümmerer 1973) and the other from the solution of a modified Orr–Sommerfeld equation for which the growth of the boundary layer is, to some extent, taken into account (Barry &

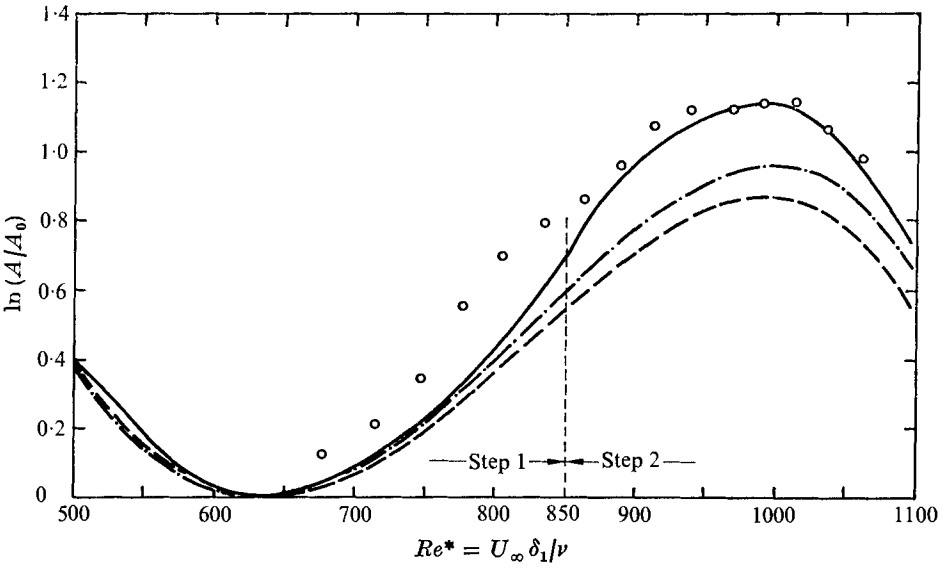

FIGURE 14. Comparison of disturbance amplification (maximum of u' perturbations) for calculation A with linear stability theory and experimental measurements. ——, numerical solution of Navier–Stokes equations; – – –, numerical solution of Orr–Sommerfeld equation; —·—·—, numerical solution of modified Orr–Sommerfeld equation; O, experimental measurements for $F = 1{\cdot}32$ (Ross *et al.* 1970).

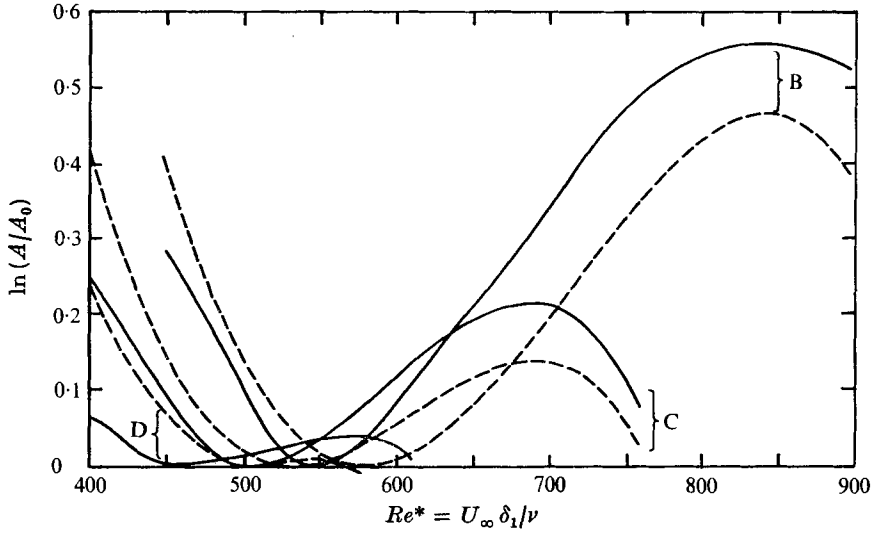

FIGURE 15. Comparison of amplification curves (maximum of u' perturbations) for calculations B, C and D with linear stability theory. ——, numerical solution of Navier–Stokes equations; – – –, numerical solution of Orr–Sommerfeld equation. B, $F = 1{\cdot}6$; C, $F = 2{\cdot}0$; D, $F = 2{\cdot}4$.

Ross 1970; Kümmerer 1973). The solution of the Navier–Stokes equations yields stronger amplification than either curve of linear stability theory and is in better agreement with the experimental measurements, especially for the second calculation step. The better agreement for the second step can possibly be explained by the fact that the perturbation profiles for the perturbation functions at the left boundary were taken from the Navier–Stokes solution at the right boundary of the calculation in step 1. The perturbation profiles for the perturbation functions in step 1 were from linear stability theory.

Amplification curves (again for the inner maximum of the u' perturbations) for calculations B, C and D are compared in figure 15 with corresponding curves from numerical solutions of the Orr–Sommerfeld equation (Jordinson 1968, 1970; Kümmerer 1973). Experimental measurements were not available for these cases. For all calculations, the Navier–Stokes solutions give again stronger disturbance amplification than linear stability theory. Moreover, the Navier–Stokes calculations lead to larger regions of instability since the neutral points (points of the amplification curves with zero slope) corresponding to the lower branch of the neutral stability curve are at lower Reynolds numbers than those of linear stability theory. (This context will become more obvious in the discussion of figure 17.)

A comparison of perturbation profiles and corresponding phase relations for a Reynolds number $Re^* = 700$ obtained from calculation A and from linear stability theory is presented in figure 16. The perturbation profiles of linear stability theory are normalized such that the maximum value of the u'_A profile is equal to the corresponding value of the Navier–Stokes calculation. The v'_A perturbation profile of the Navier–Stokes solution is somewhat below that of linear stability theory. This is consistent with the fact that different amplification rates were obtained for the different perturbation variables (figure 10). Certain deviations are also present near the locations where the phase shift occurs for the u' and ω' perturbations, since the profiles of the Navier–Stokes solution do not reach the y axis. This effect may be attributed to the possible existence of other harmonic wave components which are not excluded when the perturbation profiles are determined in the manner previously described. From experiments (Ross *et al.* 1970; see also Barnes 1966) it is known, for example, that the locations of the phase reversals for the first and second harmonic waves are not identical.

The agreement of the phase relations obtained from the Navier–Stokes calculations with those of linear stability theory is extraordinarily good, especially when considering the rather crude phase relations used for the perturbation functions at the left boundary, where no y variation was admitted at all. Thus, the Navier–Stokes solution verifies the linear stability theory phase relations which are, particularly for the ω' perturbations, rather peculiar near the wall.

Finally, in figure 17 some neutral points of the Navier–Stokes solutions are shown on a stability diagram of dimensionless frequency parameter F versus Reynolds number Re^*. These points are determined from the high and low points of the amplification curves in figures 14 and 15 for the inner maximum of the u' perturbations. For comparison, neutral points are shown which were obtained

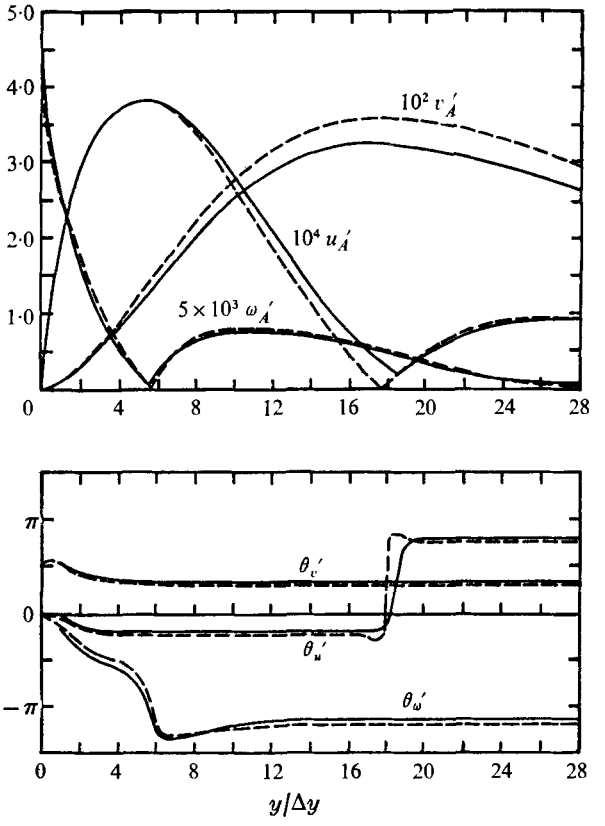

FIGURE 16. Comparison of perturbation profiles and phase relationships with linear stability theory. Calculation A, $Re^* = 700$. ——, numerical solution of Navier–Stokes equations; – – –, numerical solution of Orr–Sommerfeld equation.

experimentally by Schubauer & Skramstad (1948) and Ross *et al.* (1970). The neutral points by Schubauer & Skramstad are from measurements made at some unspecified position below the inner maximum of the root-mean-square values of the u' perturbations. The neutral points by Ross *et al.* are from measurements made at the position of the inner maximum, thus corresponding to the neutral points obtained numerically from the present Navier–Stokes calculations. The numerical results are also compared with three neutral curves of theoretical studies. One neutral curve was obtained from a numerical solution of the Orr–Sommerfeld equation (Jordinson 1970). A second curve was obtained from a numerical solution of a modified Orr–Sommerfeld equation for which additional terms, due to the vertical components of the mean flow, were included (Barry & Ross 1970; Kümmerer 1973). The third theoretical curve is the appropriate neutral curve (for the inner maximum of u') of Gaster's (1974) investigation of the effects of boundary-layer growth on stability.

For the right branch of the neutral stability curve the neutral points of the Navier–Stokes calculations agree quite well with the experimental points and the theoretical curves. For the left branch the calculated neutral points are at

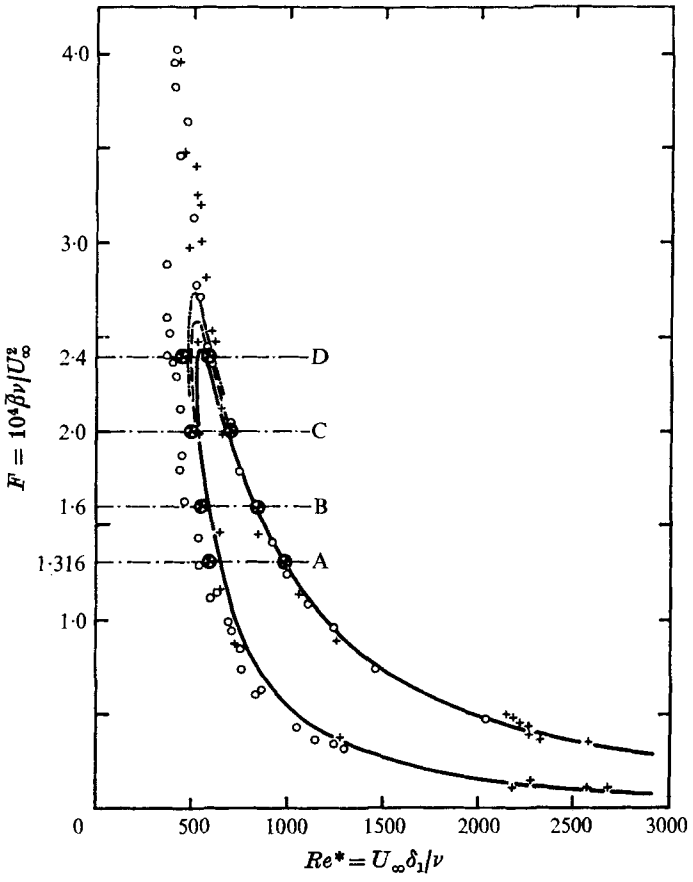

FIGURE 17. Comparison of neutral points with linear stability theory and experimental measurements. ——, numerical solution of Orr–Sommerfeld equation; – – –, numerical solution of modified Orr–Sommerfeld equation; —·—·—, numerical investigation (Gaster 1974); +, experimental measurements (Schubauer & Skramstad 1948); ○, experimental measurements (Ross *et al.* 1970); ⊗, numerical solution of Navier–Stokes equations.

somewhat lower Reynolds numbers than the theories predict and are in slightly better agreement with the experimental points of Ross *et al.* The discrepancy between experimental points and linear stability theory increases with higher disturbance frequencies, while the neutral points of the Navier–Stokes solutions seem to show a clear tendency towards the experimental points. However, more calculations with higher frequencies are required to support this speculation.

7. Conclusion

The results of the numerical calculations discussed here indicate that the presented numerical method for the solution of the Navier–Stokes equations is applicable for the investigation of stability and initial transition phenomena of incompressible, two-dimensional boundary-layer flows. The method has been subjected to critical numerical test calculations with periodic disturbances where

the results gave good agreement with linear stability theory or physical experiments. The conjecture is that this method can now be applied with some confidence to the investigation of a number of questions concerning stability and the growth of disturbances leading to transition which could not be resolved by linear stability theory. Of special interest would be, for example, a closer study of the region of instability for higher disturbance frequencies (see figure 17) where considerable discrepancy exists between experiments and linear stability theory. Further, it should be possible to investigate the influence of higher harmonic wave components, and experimentation with larger disturbance amplitudes should allow some insight into the effects of finite amplitudes on stability and transition.

This research was supported by the Deutsche Forschungsgemeinschaft, Bonn-Bad Godesberg, contract Ep 5/1-5/4.

REFERENCES

BARNES, F. H. 1966 A hot wire anemometer study of the effect of disturbances on the laminar boundary layer on a flat plate. Ph.D. thesis, University of Edinburgh.

BARRY, M. D. J. & ROSS, M. A. S. 1970 The flat plate boundary layer. Part 2. The effect of increasing thickness on stability. *J. Fluid Mech.* **43**, 813–818.

BENNEY, D. J. & LIN, C. C. 1960 On the secondary motion induced by oscillations in a shear flow. *Phys. Fluids*, **3**, 656–657.

BOUTHIER, M. 1972, 1973 Stabilité linéaire des écoulements presque parallèles. *J. Méc.* **11**, 599–621, **12**, 75–95.

CHENG, S. I. 1970 Numerical integration of Navier–Stokes equations. *A.I.A.A. J.* **8**, 2115–2122.

FASEL, H. 1974 Untersuchungen zum Problem des Grenzschichtumschlages durch numerische Integration der Navier–Stokes Gleichungen. Dissertation, University of Stuttgart.

GASTER, M. 1974 On the effects of boundary-layer growth on flow stability. *J. Fluid Mech.* **66**, 465–480.

GREENSPAN, H. P. & BENNEY, D. J. 1963 On shear-layer instability, breakdown and transition. *J. Fluid Mech.* **15**, 133–153.

HADAMARD, J. 1952 *Lectures on Cauchy's Problem in Linear Partial Differential Equations.* Dover.

JORDINSON, R. 1968 The transition from laminar to turbulent flow over a flat plate – space amplified, numerical solutions of the Orr–Sommerfeld equation. Ph.D. thesis, University of Edinburgh.

JORDINSON, R. 1970 The flat plate boundary layer. Part 1. Numerical integration of the Orr–Sommerfeld equation. *J. Fluid Mech.* **43**, 801–811.

KÜMMERER, H. 1973 Numerische Untersuchungen zur Stabilität ebener laminarer Grenzschichtströmungen. Dissertation, University of Stuttgart.

RICHTMYER, R. D. & MORTON, K. W. 1967 *Difference Methods for Initial-Value Problems.* Interscience.

ROACHE, P. J. 1972 On artificial viscosity. *J. Comp. Phys.* **10**, 169–184.

ROSS, J. A., BARNES, F. H., BURNS, J. G. & ROSS, M. A. S. 1970 The flat plate boundary layer. Part 3. Comparison of theory with experiment. *J. Fluid Mech.* **43**, 819–832.

SCHLICHTING, H. 1965 *Grenzschicht-Theorie*, 5th edn. Karlsruhe: G. Braun.

SCHUBAUER, G. B. & SKRAMSTAD, H. K. 1948 Laminar boundary-layer oscillations and transition on a flat plate. *N.A.C.A. Rep.* no. 909.

STUART, J. T. 1965 Hydrodynamic stability. *Appl. Mech. Rev.* **18**, 523–531.

THOMAS, L. H. 1949 Elliptic problems in linear difference equations over a network. *Watson Sci. Comp. Lab. Rep., Columbia Univ., New York.*

WAZZAN, A. R., OKAMURA, T. T. & SMITH, A. M. O. 1968 Spatial and temporal stability charts for the Falkner–Skan boundary-layer profiles. *McDonnell-Douglas Astronautics Co., Rep.* no. DAC-67086.